Thermal Modeling of Mini-Channel and Laminated Types Evaporator in Mobile Air Conditioning System

S. Sanaye* and M. Dehghandokht

[1] Associated Professor, [2] P.hD Student, Energy Systems Improvement Laboratory (ESIL) Department of Mechanical Engineering Iran University of Science and Technology (IUST)

* sepehr@iust.ac.ir

Abstract

In this paper, mini-channel type evaporator which is new in mobile air conditioning (MAC) or automotive air conditioning (AAC) systems is thermally modeled. The performance of mini-channel evaporator is also compared with the laminated evaporator which is being currently used in automotive industries. The mini-channel evaporator was constructed of two rows of parallel flow mini-channel tubes with inlet and outlet headers. The numerical results of modeling the laminated and mini-channel evaporators validated with the corresponding experimental data which was obtained from experiments performed on mobile air conditioning system in calorimeter test bench. The comparison of modeling results of two evaporators showed good agreement with experimental data. The performance of laminated and mini-channel evaporators were also compared under various operating conditions. The mini-channel evaporator had higher cooling capacity (7.2%) and higher refrigerant pressure drop (45%) in comparison with the corresponding values in laminated evaporator assuming the same external geometry. The outlet air temperature and enthalpy of mini-channel evaporator was also lower, 11% and 8% respectively, than that for laminated evaporator. This cause to reduce the time period as well as power/fuel consumption for reaching the comfortable cabin temperature.

Keywords: "Mini-channel evaporator", "Modeling", "Laminated evaporator", "Performance"

1. INTRODUCTION

Development of compact heat exchangers with high effectiveness is one method for improving the efficiency of vapor compression refrigeration systems and reducing their environmental impact by lowering the power consumption to provide specific cooling effect. According to Kandlikar's heat transfer tube classification, the hydraulic diameter (D_h) range of mini-channel tube is between 0.2 mm and 3 mm (Kandlikar & Grande [1]). Mini-channel heat exchangers with D_h less than 3 mm are widely used in modern air-conditioning, heat pumps, and refrigeration systems for a variety of residential, industrial and process industry applications. One of the principal ideas behind using mini and micro (microchannels with D_h less than 0.2 mm) scales heat exchangers is their potential for enhanced heat transfer coefficients. Mini-channel tube technology is currently used in R134a automobile air conditioning systems.

Plate type evaporators are widely used as a conventional device in automotive industry. Many researchers investigated the performance of this type of evaporators. Corberán & Melón [2] and Horuz et al.

[3] developed the thermal modeling of plate type evaporator to predict the performance of this type of evaporator. Lee & Yoo [4] modeled the automobile air conditioning system using plate type evaporator. They developed a mathematical model to study the effects of various operating parameters on the performance of the plate type evaporator. Wellsandt & Vamling [5] investigated experimentally and theoretically this type of evaporators. Their modeling results had a good accuracy in comparison with the experimental tests.

The mini-channel heat exchangers are more compact and have higher heat transfer rate in comparison to the conventional compact heat exchangers such as plate type heat exchangers for the same external geometry. Since mini-channel heat exchangers have much less internal volume than the conventional compact heat exchangers, the system using mini channel evaporators requires less refrigerant charge.

The Modeling of the mini-channel heat exchangers is investigated by several researchers. Yin et al. [6] developed a CO_2 mini-channel gas cooler model. In their model, each pass was separated into 10 equal-length element. The model predicted the gas cooler capacity with a good accuracy. Asinari et al. [7]

developed a mini-channel gas cooler model based on predicting the hot and cold sides flow convection heat transfer coefficients. They reported that the accuracy of modeling results of evaporator cooling capacity prediction could be improved if thermal conduction inside metal was included in the gas cooler model. Shao et al. [8] developed a numerical model for serpentine mini-channel condenser. The results of their modeling showed a good match with experimental results.

The number of literature on thermal modeling of mini-channel evaporators is not too many. Kim & Bullard [9] developed a model for CO_2 microchannel evaporator. The model was based on using the finite volume analysis of air-side heat and mass transfer processes. They neglected the tube wall thermal resistance in the proposed model. Qi et al. [10] experimentally studied the mini-channel evaporators in a refrigeration system test bench and compared the results of two mini-channel and conventional laminated evaporators (compact heat exchangers with hydraulic diameter bigger than 3 mm) in mobile air conditioning system.

In this paper, the thermal modeling of mini-channel and laminated evaporators for applications in automotive industry were performed. The modeling results validated by the results of empirical tests for both mentioned kinds of evaporators. The advantages of mini-channel evaporator in comparison with laminated evaporator are discussed.

The contributions of this paper with the subject are:
- Proposing a new form of modeling mini-channel evaporators applying overall heat transfer coefficient and ε-NTU method for both wet and dry air conditions.
- Improving the modeling results with the experimental tests performed in the hot test room at various operating conditions.

2. THERMAL MODELING OF AUTOMOTIVE EVAPORATOR

The laminated evaporators are widely used in mobile air conditioning system (MAC). The laminated type plate-fin evaporators are constructed as a sandwich of U-type plates and internal fins to enhance refrigerant side heat transfer with louver fins in between the plates. The refrigerant and air are carried between alternate pairs of plates in cross flow. Figure

1 shows this type of evaporators.

The new design of evaporators namely mini-channel was used by automotive industries. Figure 2 shows the schematic diagram of mini-channel evaporator which is composed of louver fins and mini-channel flat tubes. There are two rows of parallel flow mini-channel tubes with inlet and outlet headers in this design. The refrigerant flowing to the flat tube is divided to mini-channel tubes (Figure 2(b)) in order to enhance refrigerant heat transfer coefficient.

The main shortcoming of laminated evaporator is its complicated manufacturing process and huge tooling fees [11]. The tooling machine for the plate and internal fins (refrigeration side) should be specially designed. Therefore the dimensions (such as length, width, height and thickness) of the plate as well as the internal fin geometry and specifications
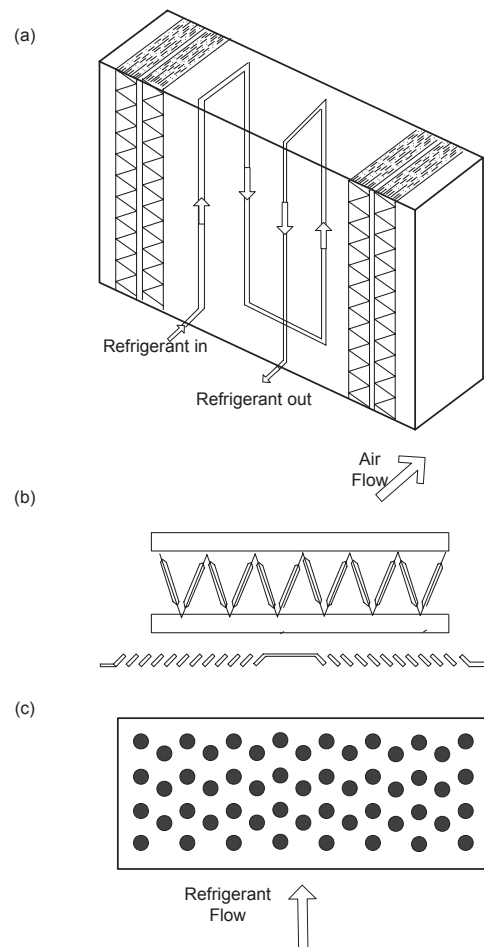

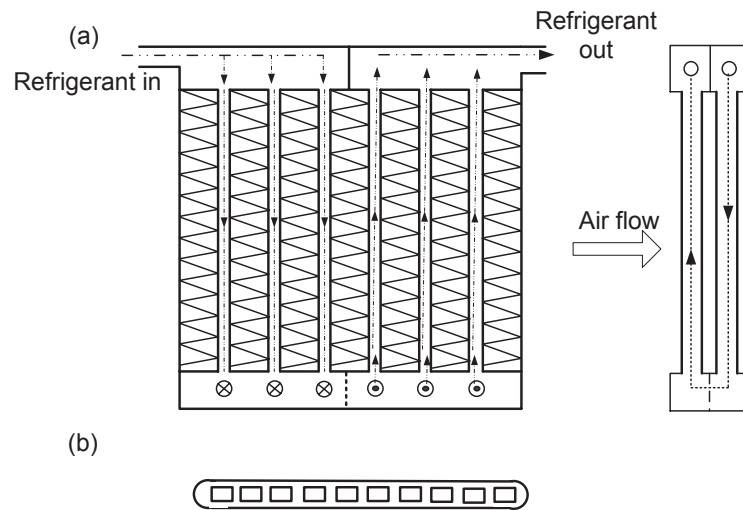**Fig. 1.** Typical structure of laminated type evaporator

Fig. 2. The schematic view of a parallel flow evaporator. (a) Front view of parallel flow evaporator. (b) mini-channel cross sections

change from one evaporator to another. This is while that the length of evaporator and mini-channel tubes in mini-channel evaporators could be changed easily by their adjusting as well as their cutting.

ε-NTU method was used for thermal analysis of ACC evaporator in this paper. Two wet and dry cases of air flow through the evaporator were investigated. When the refrigerant temperature was below the air dew point temperature, the process was named "wet condition" for which, air water vapor condensation occurs. Special concerns such as using air enthalpy instead of air temperature and latent heat in heat exchanger analysis should be taken care of when ε-NTU relations are used in wet condition. In "dry condition", the refrigerant temperature is above the dew point temperature.

It was assumed that the distribution of refrigerant in the mini-channels of flat tubes is uniform.

In order to exert the ε-NTU relations, flat tubes in each pass were divided into number of elements equal to the number of air fins each was named the kth element.

3. ε-NTU METHOD UNDER DRY CONDITION [12]

The heat transfer rate from the kth element under dry condition is:

$$\left(Q = \varepsilon C_a (T_{r,i} - T_{a,i}) \right)_k \tag{1}$$

For single-phase regions (superheat), ε the

effectiveness may be explained as:

$$\varepsilon = 1 - \exp\left[(\frac{1}{C^*})(NTU)^{0.22} \left\{ \exp(-C^*(NTU)^{0.78} - 1) \right\} \right] \tag{2}$$

For two-phase regions (saturation condition including evaporation), ε is:

$$\varepsilon = 1 - \exp(-NTU) \tag{3}$$

where the number of transfer units and their corresponding parameters are:

$$NTU = \left(\frac{UA}{C} \right)_a \tag{4}$$

$$C^* = \frac{C_a}{C_r} \tag{5}$$

$$C_r = \dot{m}_r c_{p,r} \tag{6}$$

$$C_a = \rho_a \dot{V}_a c_{p,a} \tag{7}$$

The overall heat transfer coefficient (UA) was obtained from:

$$\frac{1}{U_a A_a} = \frac{1}{\eta_f h_a A_a} + \frac{1}{A_r h_r} \tag{8}$$

where the fin efficiency (η_f) was:

$$\eta_f = \frac{\tanh\left(\left(\frac{F_h}{2} - t_f\right)\sqrt{\frac{2h_a}{k_f t_f}\left(1 + \frac{t_f}{F_d}\right)}\right)}{\left(\frac{F_h}{2} - t_f\right)\sqrt{\frac{2h_a}{k_f t_f}\left(1 + \frac{t_f}{F_d}\right)}} \tag{9}$$

4. ε-NTU METHOD UNDER WET CONDITION [13]

The heat transfer rate from the kth element under wet condition is:

$$\left[Q = \varepsilon Q_{i,max}\right]_{k,w} \tag{10}$$

$$\left[Q_{max} = \dot{m}_a.(i_{a,i} - i_{s,r,i})\right]_{k,w} \tag{11}$$

Where k and w denotes for the kth element and wet condition respectively.

For single-phase (superheat) and two phase (saturation-evaporation) regions, the estimation of effectiveness in wet condition had the same relations as equations 2 and 3 respectively.

Therefore the number of transfer units and their corresponding parameters under wet condition are:

$$NTU = \frac{(U_a A_a)_w}{C_{min}} \tag{12}$$

$$C^* = \frac{C_{min}}{C_{max}} \tag{13}$$

$$C_{min} = Min(C_1, C_2) \tag{14}$$

$$C_{max} = Max(C_1, C_2) \tag{15}$$

$$C_1 = \dot{m}_a \tag{16}$$

$$C_2 = \dot{m}_r \tag{17}$$

Where the wet overall heat transfer coefficient $(U_a A_a)_w$ was obtained from:

$$\left(\frac{1}{U_a A_a}\right)_w = \frac{b_w}{\left(1 - \frac{A_f}{A_a}\left(1 - \eta_{f,w}\right)\right)h_{a,w} A_a} + \frac{c_{p,r}}{A_r h_r} \tag{18}$$

where the fin efficiency ($\eta_{f,w}$) under wet condition is:

$$\eta_{f,w} = \frac{\tanh\left(\left(\frac{F_h}{2} - t_f\right)\sqrt{\frac{2h_{a,w}}{k_f t_f}\left(1 + \frac{t_f}{F_d}\right)}\right)}{\left(\frac{F_h}{2} - t_f\right)\sqrt{\frac{2h_{a,w}}{k_f t_f}\left(1 + \frac{t_f}{F_d}\right)}} \tag{19}$$

$$h_{a,w} = \frac{1}{\frac{c_{p,a}}{b_w}\left(\frac{1}{h_a} + \frac{k_w}{y_w}\right)} \tag{20}$$

where y_w/k_w is the thermal resistance (0.1 m².KW⁻¹ in this paper) of water droplets generated on the evaporator air side fins [9].

5. AIR SIDE HEAT TRANSFER AND PRESSURE DROP COEFFICIENTS

The air side convection heat transfer coefficient (h_a) for the flow over the louver fins was computed from [14]:

$$h_a = \frac{0.26712\, Z Re\; k_a\, Pr_a^{\frac{1}{3}}\, Re_{Lp}^{-0.1944}}{D_{h,a}} \tag{21}$$

where the Z is defined as:

$$Z = \left(\frac{L_a}{90}\right)^{0.0257}\left(\frac{F_h}{L_p}\right)^{-1.9045}\left(\frac{L_h}{L_p}\right)^{1.7159}$$

$$\left(\frac{F_p}{L_p}\right)^{-0.5177}\left(\frac{F_d}{L_p}\right)^{-0.2127}\left(\frac{t_f}{L_p}\right)^{-0.05} \tag{22}$$

In order to calculate the air side pressure drop, the f factor for flow over the louver fins was computed from [14]:

$$f = 0.54486\, Re_{LP}^{-0.3068}\left(\frac{L_a}{90}\right)^{0.444}\left(\frac{F_h}{L_p}\right)^{0.5458}$$

$$\left(\frac{L_h}{L_p}\right)^{-0.2003}\left(\frac{F_p}{L_p}\right)^{-0.9925}\left(\frac{F_d}{L_p}\right)^{0.0688} \tag{22}$$
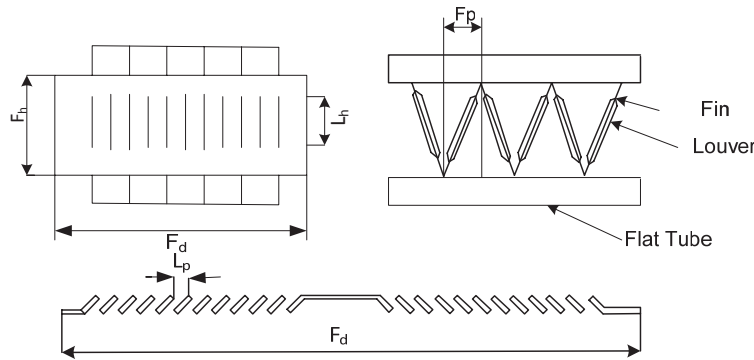
Fig. 3. The schematic view and geometrical parameters of louver fins

Then the pressure drop was estimated from:

$$\Delta P = f \frac{F_d}{D_{h,a}} \rho_a \frac{V^2}{2} \tag{24}$$

The parameters used in equations. (21), (22), (23) and are illustrated in Figure 3.

6. REFRIGERANT SIDE HEAT TRANSFER COEFFICIENT

6. 1. Single Phase Flow

For the laminated evaporator, heat transfer in the refrigerant plates is enhanced by fins. The geometry of fins resembles elongated dimples (Figure 1(c)). For this type of plates, the refrigerant heat transfer coefficient at single phase region is obtained from [15].

$$h_r = 0.02106 \frac{k}{D_h} Re_{D_h}^{0.62} Pr^{\frac{1}{3}} \tag{25}$$

The D_h for plate evaporators as shown in Figure 1(a) is defined as [16]:

$$D_h = \frac{4s_f h_f L_f}{2(s_f L_f + h_f L_f + t_f h_f) + t_f s_f} \tag{26}$$

For mini-channel tube, the refrigerant side convection heat transfer coefficient is [17]:

$$h_r = 0.023 Re_{D_h}^{0.8} Pr^{0.3} \frac{k}{D_h} \tag{27}$$

6. 2. Two Phase Flow

For laminated plates, the two phase heat transfer coefficient was based on correlations proposed in [18]. The two phase heat transfer coefficient is the larger of either the nucleate boiling or convective boiling heat transfer coefficient. These heat transfer coefficient are determined as follows.

$$h_{NB} = 0.6633 CO^{-0.2} (1-x)^{0.8} h_{lo} E_{CB} +$$

$$E_{CB} + 1058 BO^{0.7} (1-x)^{0/8} F_{fl} h_{lo} E_{NB} \tag{28}$$

$$h_{CB} = 1.136 CO^{-0.9} (1-x)^{0.8} h_{lo} E_{CB} + \text{(}$$

$$66.7 BO^{0.7} (1-x)^{0.8} F_{fl} h_{lo} E_{NB} \tag{29}$$

E_{fl} is a fluid dependent parameter that is equal to 1.63 for R134a. The definition of convection number, Co, and boiling number are as follows:

$$CO = \left(\frac{\rho_v}{\rho_l}\right)^{0.5} \left(\frac{1-x}{x}\right)^{0.8} \tag{30}$$

$$BO = \frac{Q_i / A_r}{G h_{fg}} \tag{31}$$

Kandlikar determined that augmentation factor for convective boiling, E_{CB} and nucleate boiling, E_{NB}, is 1.2 and 0.77 respectively.

For mini channel tubes, the two phase heat transfer coefficient is [19]:

$$h_r = 770\left(Bo\,Re_{D_h}(1-x)N_{conf}\right)^{0.62}\left(\frac{\rho_v}{\rho_l}\right)\left(\frac{k_l}{D_h}\right) \quad (32)$$

where:

$$N_{conf} = \frac{1}{D_h}\left(\frac{\sigma}{g(\rho_l-\rho_v)}\right)^{0.5} \quad (33)$$

7. REFRIGERANT PRESSURE DROP

7. 1. Laminated Plate Type

Due to the complicated plate-fin geometry and no published documentation for frictional pressure drop for this type of geometry, the pressure drop of laminated plate fin type of evaporator was measured experimentally.

The refrigerant pressure drop in evaporator versus vapor Reynolds number (Re_g in Eq. 31) is plotted in Figure 4:

$$Re_g = \frac{x\dot{m}_r D_h}{\mu_g A} \quad (34)$$

where x is the inlet refrigerant quality and D_h is the hydraulic diameter. It is quite noteworthy that the pressure drop under various operating conditions can be expressed in terms of only one parameter, the Reynolds number:

$$\Delta P = A\,Re_g^B \quad (35)$$

A and B were obtained experimentally.

7. 2. Mini-Channel Tube

The pressure drop relations for the refrigerant side

in the parallel multi-channel flat tube evaporator in single and two-phase regions are:
For single-phase region [20]:

$$\Delta P = 2f\frac{L}{D_h^3}\frac{\mu_l^2}{\rho_l}Re_{Dh}^2 \quad (36)$$

where L is the fin length along the refrigerant flow.

$$Re_{Dh} = \frac{GD_h}{\mu} \quad (37)$$

f, the friction coefficient for single-phase region was:

$$f = 0.079\,Re_{D_h}^{-0.22} \quad (38)$$

The pressure drop for two-phase (boiling) region was [21]:

$$\Delta P = \Delta P_{lo}\phi_{lo}^2 \quad (39)$$

where ΔP_{lo} is the pressure drop for treating the total two phase mixture as liquid alone.

$$\Delta P_{lo} = \frac{2f_{lo}G^2L}{\rho_l D_h} \quad (40)$$

where f_{lo} is the friction factor for treating the total two phase mixture as liquid alone [22].

$$f_{lo} = (0.79\,Re_{lo}-1.64)^{-2} \quad (41)$$

The two phase multiplier, , is expressed as [21]:

$$\phi_{lo}^2 = 1+\left(4.3\Gamma^2-1\right)\left[N_{conf}x^{-0.875}(1-x)^{0.875}+x^{1.75}\right] \quad (42)$$

where:

Fig. 4. Variation of pressure drop with the Reynolds number in the laminated evaporator

$$\Gamma = \left(\frac{\rho_l}{\rho_v}\right)^{0.5}\left(\frac{\mu_v}{\mu_l}\right)^{0.125} \tag{43}$$

8. THE EXPERIMENTAL SET UP

A group of tests were conducted and the measured data were obtained to validate the evaporator thermal modeling. Two types of evaporators, laminated and mini-channel, with the specific dimensions and geometries were tested in the experimental set-up and their operating parameters were measured under various designed conditions.

The test set-up of AAC system included: an evaporator, condenser, compressor, expansion valve. As is shown in Figure 5, the test set-up included three circuits: refrigerant, the air flowing through the condenser, and the air flowing through the evaporator. The required air to flow through the condenser was provided by a turbofan. The velocity of the air flow through the condenser was controlled by the nozzles, and the condenser inlet air temperature was controlled by a heater installed at the condenser down stream. The refrigerant mass flow rate was controlled by a thermal expansion valve. The compressor clutch only turns the compressor on and off. The refrigerant used in the empirical test set-up was R-134a.

For the evaporator in the test room, the sensible thermal load was provided by a heater, and the non-sensible thermal load was provided by a humidifier installed at the evaporator down stream. The refrigerant temperature, pressure, and mass flow rate were measured at locations shown in Figure 5. The refrigerant mass flow rate was measured by a Coriolis meter located at liquid refrigerant region. The thermometers were T type thermocouple, and barometers were pressure transducers. The compressor rotational speed and torque were measured by a tachometer and torque meter respectively. The accuracy of measuring devices is listed in Table 1.

To perform the tests, the evaporator input parameters were applied in the system settings and the evaporator output (operating) parameters were adjusted after reaching the steady state condition.

Table 1. The accuracy of measuring devices

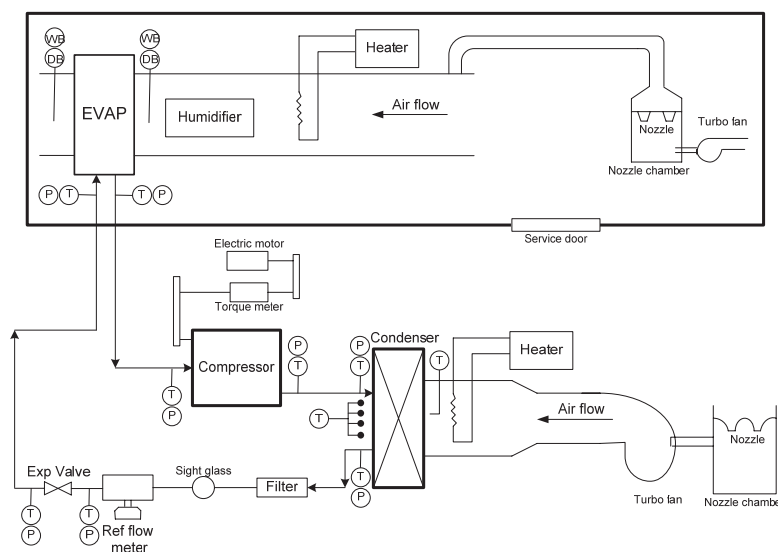| ITEM	RANGE	PRECISION
Refrigerant mass Flow Rate	0- 400 kg/h	1 kg/h
Air volume flow rate	200-700 m³/h	0.5 m³/h
Rotational Speed	0- 5000 RPM	±40 RPM
Torque	0- 50 N.m	±0.1 N.m
Thermocouple	0- 100°C	±0.4°C
Pressure Transducer	80- 3500 kPa	±10 kPa

Fig. 5. A schematic view of evaporator test set-up

The evaporator steady state condition reached when the heat transfer rate of refrigerant and air sides were matched with the difference percent points of less than 5%.

The refrigerant and air side heat transfer rates were computed from the following equations:

$$\dot{Q}_r = \dot{m}_r \left(h_{r,o} - h_{r,i} \right) \tag{44}$$

$$\dot{Q}_a = \rho u_a A \left(h_{a,i} - h_{a,o} \right) \tag{45}$$

The reported heat transfer rate is:

$$\dot{Q}_{exp} = \frac{\dot{Q}_a + \dot{Q}_r}{2} \tag{46}$$

9. DISCUSSION AND RESULTS

9. 1. Algorithms for Thermal Modeling

Based on relations mentioned in section (2), the flow chart of modeling procedure was developed as is shown in Figure 6. The input parameters into the evaporator model could be divided into two main
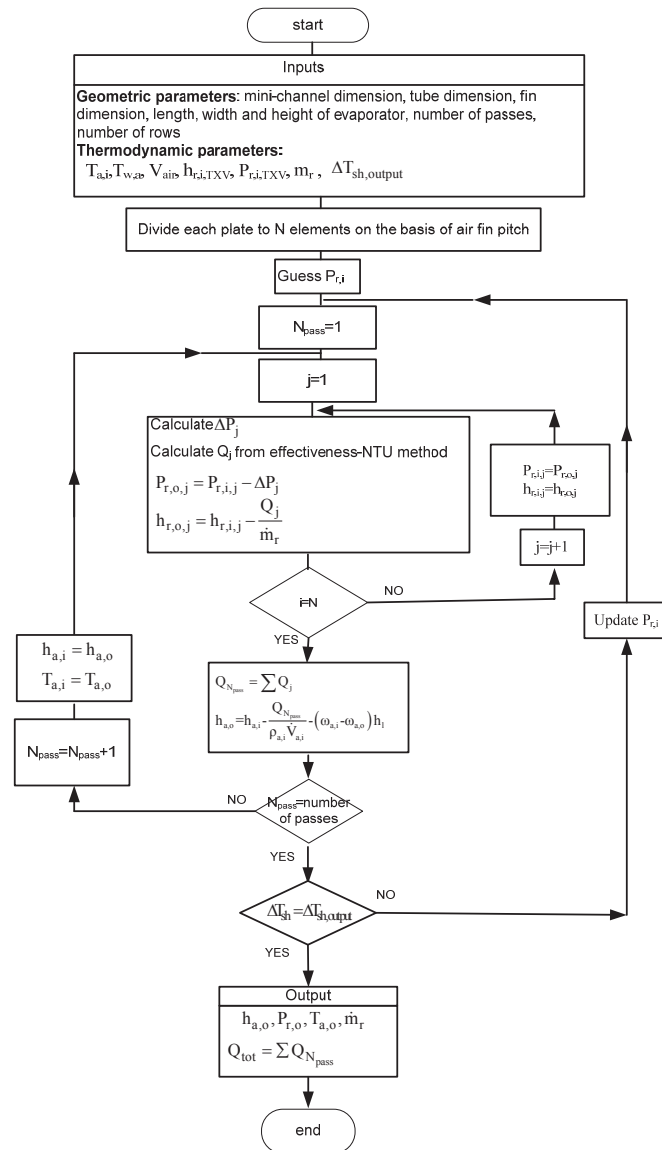

Fig. 6. Flowchart for the modeling of evaporator

groups:

1. Geometric parameters such as length, width and high of evaporator, air fin dimensions, flat tube dimensions, mini-channel dimension, number of tubes (plates) in each pass of evaporator and number of passes.

2. Thermodynamic parameters such as evaporator inlet air dry and wet bulb temperatures ($T_{a,i}$, $T_{w,a,i}$), air volume flow rate flowing through evaporator (V_a), expansion valve inlet refrigerant pressure ($P_{r,i,TXV}$), and enthalpy ($h_{r,i,TXV}$), refrigerant mass flow rate ($\dot{m}_r$), and degree of superheat of refrigerant flowing out the evaporator ($\Delta T_{sh,output}$).

In real situation the AAC system has a dynamic operational mode. Therefore the expansion valve adjusts the mass flow rate of refrigerant into evaporator ($\dot{m}_r$) such that to keep the constant degree of superheat at the evaporator outlet. By knowing pressure and enthalpy flowing in to expansion valve, the refrigerant enthalpy at the evaporator inlet was known. This was while the process of flowing refrigerant through the expansion value was considered to be isenthalpic. To estimate the heat transfer rate and pressure drop, each pass of evaporator was divided in to many number of elements (j) equal to the number of air-fins. Then heat transfer rate and pressure drop were estimated in each element from ε-NTU method and the exit refrigerant enthalpy and the exit air temperature in each element were obtained. During these computations the locations of one-phase (compressed liquid and superheat) as well as two-phase (saturated) regions of refrigerant were detected.

The evaporator heat transfer rate in each pass was the sum of heat transfer rate in each element and the total heat transfer rate in one pass was the sum of heat transfer rates of all elements in each pass. The dry bulb temperature and enthalpy of air at the exit of each pass was computed by using mass and energy balance equations for the air flow.

With computing the heat transfer rate for all elements of passes in evaporator, the refrigerant pressure and enthalpy were obtained at the evaporator exit with the known adjusted superheat degrees. The modeling procedure starts with guessing the evaporator inlet refrigerant pressure and finds the final value of this parameter by try and error procedure to

satisfy the adjusted evaporator exit superheating degrees. At this point, the output operating parameters such as evaporator outlet refrigerant pressure ($P_{r,o}$) and temperature ($T_{r,o}$), evaporator outlet air temperature ($T_{a,o}$) and enthalpy ($h_{a,o}$) as well as the total heat transfer rate ($\dot{Q}$) and pressure drop (ΔP) were estimated and saved as the final results. Otherwise with the new inlet refrigerant pressure in evaporator, the mentioned procedure was repeated.

10. UNCERTAINTY ANALYSIS

The experimental uncertainty analysis was carried out based on concepts and relations given in [23]. Errors from the measured primary parameters propagate into the secondary variables depending on their relationships. If A is a secondary parameter, which depends on other primary measured parameters such as A1, A2, and A3, then the errors from the measured primary parameters propagate into the secondary parameter A according to the relationship between A and A1, A2, and A3. The absolute uncertainty of A (UA) is then calculated using root sum square (RSS) method as expressed by equation 47.

$$U_A = \sqrt{\left(\frac{\partial A}{\partial A_1} U_{A_1}\right)^2 + \left(\frac{\partial A}{\partial A_2} U_{A_2}\right)^2 + \ldots \ldots} \qquad (47)$$

The partial derivatives $\frac{\partial A}{\partial A_1}$, $\frac{\partial A}{\partial A_2}$, $\frac{\partial A}{\partial A_3}$ ... of the secondary or dependent parameters are derived from their relationship with the primary or independent parameters.

The individual uncertainties of the independent parameters U_{A1}, U_{A2}, U_{A3} are estimated from the bias and precision of both the experimental and instrument (Table 1) errors. The relative uncertainty is generally obtained by dividing the absolute uncertainty by the mean value as shown in equation 48.

$$\frac{U_A}{A} = \frac{\sqrt{\left(\frac{\partial A}{\partial A_1} U_{A_1}\right)^2 + \left(\frac{\partial A}{\partial A_2} U_{A_2}\right)^2 + \ldots \ldots}}{f\left(A_1, A_2, \ldots\right)} \qquad (48)$$

The estimated relative uncertainties for the refrigerant pressure drop of laminated type evaporator obtained from experimental results (equation 34), heat transfer rate and enthalpy of air in the current study are tabulated in Table 2.

Table 2. Relative uncertainty of key parameters

parameter	Uncertainty
Pressure drop (ΔP)	6.1%
Heat transfer rate (Q)	4.3%
Enthalpy of air (i_a)	2.2%

Table 3. Experimental test operating conditions

Parameter	Range
$T_{a,i}$ (C)	20-50
$T_{w,a,i}$ (C)	14-40
$\dot{V}_a$ (m^3/h)	300-500
$P_{r,i}$ (kPa)	270-600
$\Delta T_{SH,o}$ (C)	5-10

11. MODEL VERIFICATION

To validate the presented model, two types of evaporators with the characteristics presented in Table 3 were designed, manufactured and tested. The modeling results were compared with the experimental results under various operating conditions (Table 4).

The results of modeling and estimating the heat transfer rate for two types of evaporators were valid within 10% range with of experimental data (Figure 7). The maximum difference between the modeling results for pressure drop and the experimental values of measured pressure drop was 12% (Figure 8). Figure 9 shows that the results for refrigerant mass flow rate obtained from the evaporator modeling agreed within

Table 4. The detail geometry of mini-channel and the laminated evaporators

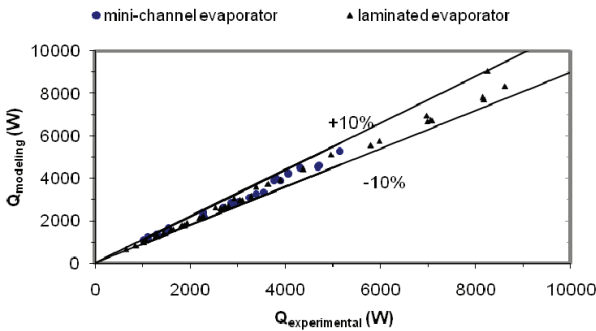| Evaporator Type	Laminated	Mini-channel
Core volume (m^3)	0.003	0.002
Face area (m^2)	0.0405	0.0408
Tube/Plate size	41 mm × 3.3 mm	19 mm × 1.7 mm- 14 holes
Fin Height (mm)	7.9	5.8
Fin pitch (mm)	2.1	2.6
Louver height (mm)	6.3	4.5
Louver pitch (mm)	1.3	1.3
Louver angle (°)	30	30
Weight (kg)	2.4	1.92

Fig. 7. Comparison of modeling and experimental evaporator heat transfer rates for mini-channel and laminated evaporators

Fig. 8. Comparison of modeling and experimental evaporator refrigerant side pressure drop for mini- channel and laminated evaporators

Fig. 9. Comparison of modeling and experimental refrigerant mass flow rate passing through the mini-channel and laminated evaporators
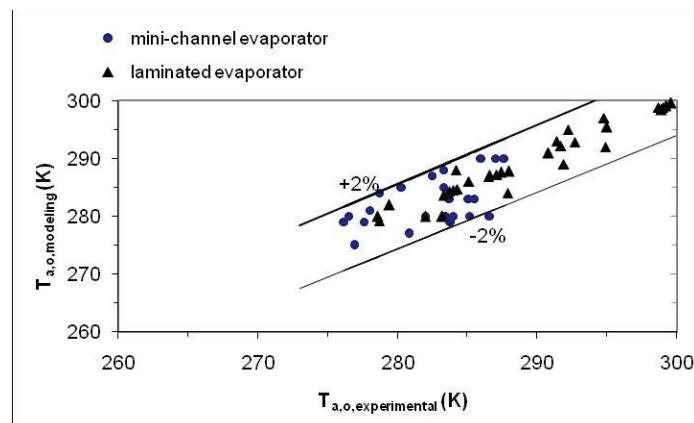

Fig. 10. Comparison of modeling and experimental evaporator outlet air temperature for mini-channel and laminated evaporators

8% range of experimental data. Figures 10 and 11 show the comparison of computed modeling results with experimental values for the air temperature and enthalpy at the evaporator outlet respectively. Evaporator exit air temperature and enthalpy are important parameters for predicting the inside cabin

air temperature. Figures 10 and 11 show that the model predictions are in good agreement with experiment values in the range of 2% and 6% for outlet evaporator air temperature and enthalpy respectively.

These results show that the numerical values of operating parameters obtained from the model under various condenser operating conditions are reliable with a reasonable accuracy.

Mini-channel evaporator performance in comparison with laminated evaporator performance

Figure 12 shows the evaporator heat transfer rate versus air volume flow rate for laminated and mini-channel evaporators with the same input operating conditions. The input parameters of this comparison are listed in Table 5. The frontal surface areas of two evaporators are almost the same while the core volume of the mini-channel evaporator was two-third

of the laminated evaporator with lower weight (80%).

Based on modeling results (equations 1 and 11), with increasing the air volume flow rate passing through evaporator, the heat transfer rate was increased. Results show that the average heat transfer rate of mini-channel evaporator was about 7.2 % higher than the corresponding value of laminated evaporator for all air volume flow rates. Figure 13 compares the results of estimating the refrigerant side

Table 5. The input parameters for comparison of the performance of laminated and mini-channel evaporators

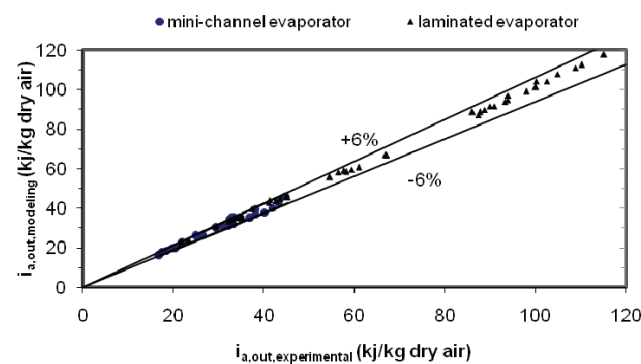| Parameter	value
$P_{r,i,TXV}$ (kPa)	2000
$T_{a,i}$ (C)	30
$T_{a,w,i}$ (C)	22
$\Delta T_{SH,o}$	5

Fig. 11. Comparison of modeling and experimental evaporator outlet air enthalpy for mini-channel and laminated evaporators
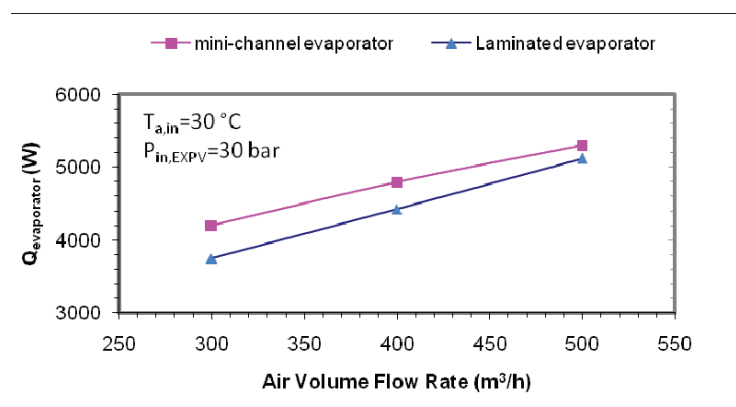

Fig. 12. Variation of evaporator heat transfer rate with the air volume flow (modeling results) for mini-channel and laminated evaporators
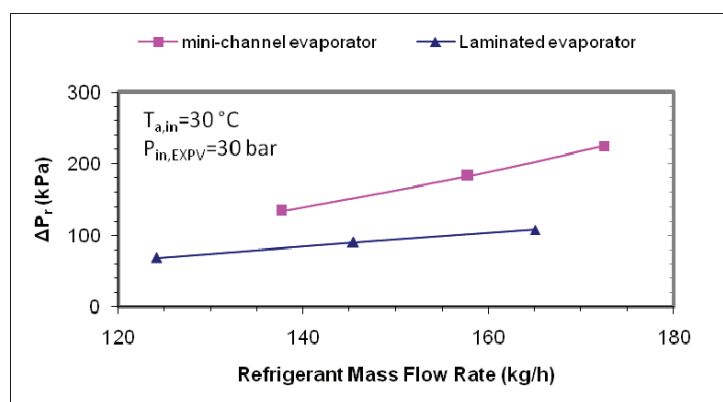
Fig. 13. Variation of refrigerant side pressure drop with refrigerant mass flow rate(modeling results) for mini-channel and laminated evaporators
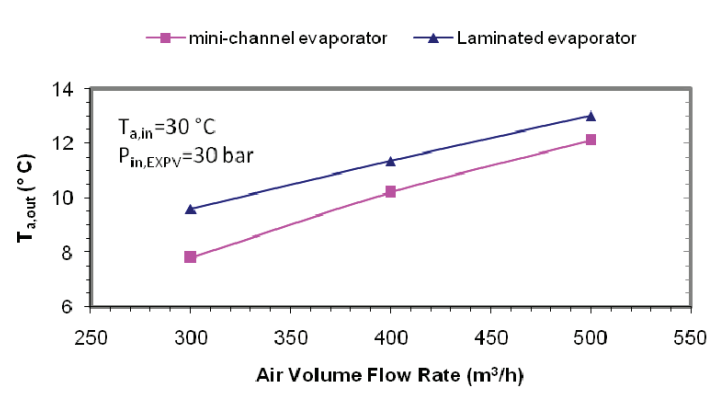

Fig. 14. Variation of evaporator air outlet dry bulb air temperature with air volume flow rate (modeling results) for mini-channel and laminated evaporators

pressure drop for two types of evaporators. The mini-channel evaporator showed an average 45% higher pressure drop than that of laminated evaporator for all refrigerant mass flow rates (this increases the compressor power consumption while cycle COP=cooling capacity/compressor power increases).

The outlet air temperature and enthalpy are important parameters for predicting the inside cabin air temperature. Figures 14 and 15 show the evaporator outlet air temperature and enthalpy of mini-channel and laminated types for various values of air volume flow rates respectively. As shown in Figures 14 and 15, the outlet air temperature and enthalpy for mini-channel evaporator are 11% and 8% (on average) lower than that for the laminated evaporator for various values of air volume flow rate respectively. Therefore the mini-channel evaporator reduces the inside cabin air temperature to a

comfortable degree faster than the laminated evaporator. Furthermore, the temperature sensor of on/off compressor clutching is located at the evaporator outlet air flow, hence, with faster reduction of evaporator outlet air temperature to an adjusting level, the compressor power consumption and engine fuel consumption reduce when the mini-channel evaporator in AAC are used.

12. CONCLUSION

A new type of mini-channel evaporator was thermally modeled. The performance of this mini-channel evaporator was compared with the laminated evaporator which is currently used in mobile air conditioning systems. The performance characteristics of mini-channel and laminated evaporators were validated with experimental results. The modeling
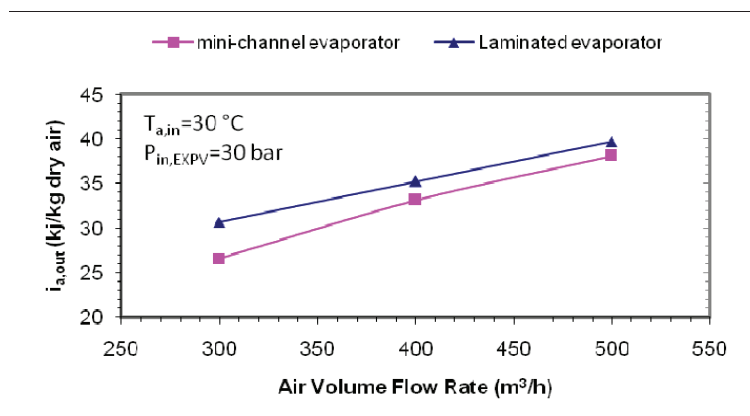
Fig. 15. Variation of evaporator air outlet enthalpy with air volume flow rate(modeling results) for mini-channel and laminated evaporators

results showed that the mini-channel heat transfer rate was higher than that of the laminated evaporator in all operating conditions. Furthermore the air exit temperature for mini-channel evaporator was lower than that for laminated one which causes to reduce the inside cabin air temperature to a comfortable degree faster when the first evaporator type were used. This provides shorter operating time and lower power consumption of compressor when mini-channel evaporator was used as well as lowers vehicle fuel consumption. The mini-channel evaporators have further advantages of 33% more compactness and 20% lighter weight than that of laminated evaporator.

Thermal modeling of evaporator helps designers to compare the performance of mini-channel evaporator with the other types of evaporators and investigate the effects of variation of design and geometrical parameters in providing the required cooling load.

13. ACKNOWLEDGEMENTS

REFERENCES

[1]   Kandlikar, S. G., Grande, W. J., "Evolution of microchannel flow passages Thermohydraulic performance and fabrication", Paper # IMECE2002-32043, Paper presented at the IMECE 2002, New Orleans, November, pp. 17–22, 2002.

[2]   Corberán, J. M., Melón, M. G., "Modeling of plate finned tube evaporators and condensers working with R134A", International Journal of Refrigeration, vol.21, pp. 273-284.

[3]   Horuz, I., Kurem, E., Yamankaradeniz, R., "Experimental and theoretical performance analysis of air-cooled plate-finned-tube evaporators", International Communications in Heat and Mass Transfer, vol.25, pp. 787-798, 1998.

[4]   Lee, G. H., Yoo, J. Y., "Performance analysis and simulation of automobile air conditioning system", International Journal of Refrigeration, vol.23, pp. 243-254, 2000.

[5]   Wellsandt, S., Vamling, L., "Heat transfer and pressure drop in a plate-type evaporator", International Journal of Refrigeration, vol.26, pp.180-188, 2003.

[6]   Yin, J. M. C. W. Bullard C. W., Hrnjak P. S., R-744 gas cooler model development and validation, International Journal of Refrigeration, vol.24, pp. 692–701, 2001.

[7]   Asinari P., Cecchinato L., Fornasieri E., Effect of thermal conduction in microchannel gas coolers for carbon dioxide, International Journal of Refrigeration, vol. 27, pp. 577–586, 2004.

[8]   Shao, L. L., Yang, L., Zhang, CL., Gu, B., "Numerical modeling of serpentine microchannel condensers", International Journal of Refrigeration, vol.32, pp. 1162-1172, 2009.

[9]   Kim, M. H., Bullard, C. W., "Development of a microchannel evaporator model for a CO_2 air-conditioning system", Energy, vol.26, pp. 931–948, 2001.

[10]   Qi, Z., Zhao, Y., Chen, J., "Performance enhancement study of mobile air conditioning system using microchannel heat exchangers", International Journal of Refrigeration, vol.33, pp. 301-312, 2010.

[11]   Sardsaz Khodro Ind. Co. technical document, 12515-59, Tehran, Iran.

[12]   Kays W. M., London A. L., Compact Heat Exchangers, third ed., McGraw-Hill, New York, 1984.

[13]   Kim, M. H., Bullard, C. W., "Air-side performance of brazed aluminum heat exchangers under dehumidifying conditions", International Journal of Refrigeration, vol.25, pp. 924–934, 2002.

[14]   Dong, J., Chen, J. , Chen, Z., Zhang, W., Zhou, Y., "Heat transfer and pressure drop correlations for the multi-louvered fin compact heat exchangers", Energy Conversion and Management, vol.48, pp. 1506-1518, 2007.

[15]   Robertson, J. M., Lovegrove, P. C., "Boiling heat transfer in brazed aluminum plate heat exchangers", ASME journal of heat transfer, vol.105, pp. 605-602, 1983.

[16]   Manglic, R. M., Bergles, A. E., "Heat transfer and pressure drop correlations for the rectangular offset strip fin compact heat exchanger Experimental and Thermal Fluid Science", vol.10, pp. 171-180, 1995.

[17]   Castro, F., Tinaut, F. V., Rahman Ali A. A., "Automotive Evaporator and Condenser Modeling", Society of Automotive Engineers, paper 931121,1993.

[18]   Kandlikar, S. G., "A model for correlating flow boiling heat transfer in augmented tubes and compact evaporators", Journal of heat transfer, vol.113, pp. 966-972, 1991.

[19]   Tran, T. N., Wambsganss, M. W., Chyu, M. C., France, D. M., "A correlation for nucleate flow boiling in small channels, in: R.K. Shah (Ed.)", Compact Heat Exchangers for the Process Industries, Begell House, New York, pp. 353–363, 1997.

[20]   Yang, C. Y., Webb, R. L., "Friction Pressure Drop of R-12 in Small Hydraulic Diameter Extruded Aluminum Tubes With and Without Micro-fins", International Journal of Heat and Mass Transfer, vol.39, pp. 805-809, 1996.

[21]   Tran, T., Chyu, M. C., Wambsganss, M., France, D., "Two-phase pressure drop of refrigerants during flow boiling in small channels: an experimental investigation and correlation development". In: Shah RK, editor. Compact heat exchangers and enhancement technology for the process industries. New York: Begell House, 1999, pp. 293–302, 1999.

[22]   Petukhov, B., "Heat transfer and friction in turbulent pipe flow with variable physical properties", Advanced Heat Transfer, vol.6, pp. 503–64, 1970.

[23]   Coleman, H. W., Steele, W. G., "Experimentation and uncertainty analysis for engineers", John Wiley & Sons, New York, 1989.

Nomenclature

A   area (m^2)

b_w slope of saturation enthalpy of moisture air versus temperature ($kjkg^{-1} K^{-1}$), $b_w = \dfrac{\Delta i_{sat}}{\Delta T_{sat}}$

c_p specific heat at constant pressure ($kjkg^{-1}K^{-1}$)

C   heat capacity rate (WK^{-1})

D   diameter (m)

E_{CB} augmentation factor for convective boiling

E_{fl} fluid dependent parameter

E_{NB} augmentation factor for nucleate boiling

F_h fin height (mm)

F_p fin pitch (mm)

F_d fin length (mm)

f   friction coefficient

g   gravitational acceleration ($m s^{-2}$)

G   mass flux ($kg m^{-2} s^{-2}$)

h   heat transfer coefficient ($W/m^{-2} k^{-1}$)

h_f fin height (mm)

h_{fg} latent heat of evaporation ($kJkg^{-1}$)

i   enthalpy ($kJkg^{-1}$)

k   thermal conductivity ($Wm^{-1}K^{-1}$)

L   length (m)

L_a louver angle (º)

L_h louver height (mm)

L_p louver pitch (mm)

$\dot{m}_r$ refrigerant mass flow rate ($kg s^{-1}$)

NTU   Number of Transfer Units

P   pressure (kPa)

P_r Prandtl number

Q   heat transfer rate (W)

Re   Reynolds number

s_f spacing between adjacent fins (mm)

T   temperature (^{o}C)

t_f fin thickness (mm)

U   overall heat transfer coefficient (Wm^{-2}K^{-2})

$\frac{U_A}{A}$ relative uncertainty (%)

u   velocity (m s^{-1})

$\dot{V}$ volume flow rate (m^3 s^{-1})

x   refrigerant quality

y_w condensetion film thickness (mm)

Greek Abbreviations

ΔP   pressure drop (kPa)

ε effectiveness

μ dynamic viscosity (Pa s)

σ surface tension (N m^{-1})

ρ density (kg m^{-3})

η_f fin efficiency

ϕ_{lo} two phase multiplier

Subscripts

a   air

CB   convective boiling

exp   experimental

f   fin

fg   saturation region

g   gas

h   hydraulic

i   inlet; inner

l   liquid

lo   liquid only

NB   nucleate boiling

o   outlet

r   refrigerant

s   saturation

TXV   Thermostatic expansion valve

v   vapour

w   wet or water